Momentum resolved joint density of state calculations for 1-dimensional electronic band structures in semiconductors

Håkon Kvernmoen

August 3, 2021

Abstract

A study on how momentum resolved joint density of state is dependent on electronic band structures along high symmetry lines. Idealized band structure models such as parabolic bands yielded good agreement with theoretical results for a direct band gap of a 1-dimensional structure. Spectra for hexagonal boron nitrite was partially recreated when compared with similar methods calculated on a 3-dimensional Brillouin zone. Additional spectra for Zinc oxide and rutile Tin(IV) oxide are calculated. By comparing minimum energy transitions for different momentum ranges, rutile Tin(IV) oxide gave qualitative agreement with values obtained by electron energy loss spectroscopy.

Contents

1 Introduction

Between the electrical conductivity of conductors and insulators we find *semiconductors*. The characteristic of these materials is the lack of an energy overlap between the valence bands (VBs) and conduction bands (CBs). In contrast to insulators, the energy difference between the valence band maximum (VBM) and conduction band minimum (CBM) is relatively small (< 5 eV [1]) and is commonly named the *band gap*. These materials, by introduction of impurities to the crystalline structure, lays the foundation for many technologies such as transistors and diodes [2] [3].

Band gaps can be divided into two main categories, *direct* and *indirect*. Direct band gaps contains transitions between the VBM and CBM where no momentum change between the two states is required, while indirect band gaps require some momentum change. One important aspect of semiconductors is the joint density of state (JDOS), where the density of possible transitions is described as a function of the energy difference between occupied and unoccupied states. In the following we will try to include momentum changes in this density description through the momentum resolved joint density of state (q-JDOS).

In understanding the q-JDOS, we will consider 1-dimensional (1D) band structures. This will not capture the full 3-dimensional (3D) band structure, but serves as a simplification where we only look at transitions along high symmetry lines in the first Brillouin zone. As an introduction we will look at different band structure models, such as pure and modified parabolic bands. This will serve as both model assessment and in understanding how different band shapes influences the q-JDOS. Thereafter we will compare with a q-JDOS calculation from [4], where the full 3D band structure of hexagonal boron nitride (h-BN) was used. By extracting the band structure along high symmetry lines, we will see how much of the full structure we can recreate.

Lastly by the use of data from the Materials project (MP) [5], band structures for different materials can be extracted. We will here be interested in two direct band gap materials, Zinc oxide (space group $P6_3mc$ in Hermann–Mauguin notation) and rutile Tin(IV) oxide ($P4_2/mmm$). These will refereed to as ZnO and r-SnO_2respectively. For r-SnO_2we will also compare the JDOS at different momentum transfers obtained by electron energy loss spectroscopy (EELS). By fitting both experimental and computed spectra for different momentum ranges, we can compare how well the two methods coincide.

2 Theory

2.1 Parabolic bands

Near the energy top of the VBs and close to the energy bottom of the CBs, we can approximate bands by parabolic functions [6]. In the 1D setting, the band energy can then be expressed as a function of the electrons wave vectors k.

$$\epsilon(k) = \epsilon_0 + \frac{\hbar^2 k^2}{2m^*} \tag{1}$$

Where ϵ_0 defines the valence band maximum (VBM) or the conduction band minimum (CBM), $\hbar$ is Planck's constant and m^* is the *effective mass* of the electron. Smaller values for m^* results in a steeper band while a larger m^* results in a flatter band. The effective mass of VBs are negative, while the effective mass of CBs are positive [6], thus giving the characteristics band structure. We will write the energy of VBs with a negative prefactor in front of the k^2 term, thus m^* is implied to be positive. Effective masses are given as fraction of the electron mas m_e. By ensuring that the CB energy is larger than the VB energy, we achieve a band gap. When referring to points in band structures, they will be gives as (k, ϵ).

2.2 Perturbations to parabolic bands

When moving away from the VBM and CBM, bands tends to diverge from the parabolic structure. One way to model this is by adding a $\epsilon(k)^2$ term that decreases the steepness of the band when moving away from the VBM or CBM. This is tuned by a parameter α with units of inverse energy.

$$\epsilon(k)(1 + \alpha\epsilon(k)) = \epsilon_0 + \frac{\hbar^2 k^2}{2m^*} \tag{2}$$

By making $\alpha \to \infty$ the bands will become flatter and more linear when moving away from the VBM/CBM, while $\alpha \to 0$ reduces to the parabolic shape from eq. (1).

2.3 Distribution of states

Electrons being Fermions, the distribution of states in the VBs and CBs will follow Fermi-Dirac statistics [7]. The probability of an available state being occupied as a function of energy is.

$$f(\epsilon) = \frac{1}{1 + e^{(\epsilon - \epsilon_f)/k_B T}} \tag{3}$$

Where k_B is the Boltzmann constant and T the temperature. ϵ_f is the Fermi-energy and decides the energy level where half of the available states can be occupied by an electron. For semiconductors the Fermi-energy lies in the band gap, thus making the VB highly populated with electrons, while the CB contains few. We will look at transitions happening at absolute zero. Thus all states below ϵ_f will be occupied by an electron, $\epsilon - \epsilon_f < 0 \Rightarrow f(\epsilon)_{T=0} = 1$ and all states above ϵ_f will be empty, $\epsilon - \epsilon_f > 0 \Rightarrow f(\epsilon)_{T=0} = 0$. This results in completely occupied VBs and completely empty CBs.

2.4 Momentum resolved joint density of state

This report is mostly concerned with the momentum resolved joint density of state (q-JDOS). Mathematically, this can be expressed as [4].

$$J(\omega, q) = \sum_{knn'} \delta(\hbar\omega - (\epsilon_{k+q,n'} - \epsilon_{k,n})) \tag{4}$$

$$\tag{5}$$

Where $\epsilon_{k,n}$ is the energy of an occupied state and $\epsilon_{k+q,n'}$ is the energy of an unoccupied state, with an additional change in wave vector q between the two states. The index n goes over every occupied state, n' goes over every unoccupied state and k goes over every wave vector. J describes the density of state at a specific energy difference $\hbar\omega$ and a specific momentum transfer $\hbar q$. Note that both k and q will be referred to as the momentum and momentum transfere respectively, keeping in mind these quantities should be multiplied by a factor of $\hbar$. There is also a possible influence of matrix elements of the form $\langle\psi_{k+q,n'}| e^{iq\cdot r} |\psi_{k,n}\rangle$, giving the transition probability between two states. This is mostly used for predicting EEL spectra and is thus neglected here. Therefor in our model every possible transition will be regarded as equally probable. When referring to points in the q-JDOS they will expressed as (q, E) with E being the energy difference between two states.

3 Method

3.1 q-JDOS implementation

There are multiple approaches to calculate the q-JDOS from eq. (5). Here we implement a energy and momentum binning approach, where we consider a discrete set of energy and momentum points with δE and δq as their respective bin sizes. Every transition is then calculated and added to its respective bin. The parameters δE and δq must be initialized before the q-JDOS is calculated and determines how similar two states has to be in the (q, E) space to be considered equal. In addition we add energy and momentum limits to our calculation, such that desired energy and momentum ranges can be extracted. In appendix B a short pseudo code of this approach is presented.

This approach does bring on some numerical problems, as the calculated q-JDOS spectrum will be dependent on the δE and δq bin sizes. Having them too large will make finer details disappear, while too small will inevitably be computationally impractical. In general we aim for bin sizes in the range $10^{-2} - 10^{-3}$ eV/Å^{-1}, dependent on how large energy and momentum limits we consider. To compensate for larger energy and momentum bin sizes, we apply a Gaussian smoothing filter after $J(\omega, q)$ is calculated.

3.2 Ideal band structures and model evaluation

Using the band structure models from eq. (1) and eq. (2), we can make a large amount of different band structures. By changing band placements, effective masses and adjusting other parameters we can in a controlled manner see how different band shapes influence the q-JDOS. In addition we can add multiple bands and try both direct and indirect band gaps. It should be noted that the q-JDOS spectrum is dependent on the range of k-points used for band generation, where increasing the k-range will allow for larger q transitions. When only considering transitions between states in the first Brillouin zone, there will be some maximum allowed q transition from the Γ points to some other point at the edge of the zone. Therefor k ranges are not set to span above the q limits used in the respective q-JDOS calculations and are centered around important features such as band gaps.

Some sort of model assessment is important to examine if the approach presented here works as intended. Using the the 1D JDOS for $q = 0$, we can run the q-JDOS algorithm on a set of parabolic bands with a direct band gap. Following the derivation from appendix A, we aim to investigate how close the calculated spectrum follows the inverse square root. Since we are working on a discrete spectrum where intensities are completely dependent on the number of k-points used for the bands, we only aim to evaluate using the proportionality:

$$\text{JDOS} \propto (E - E_g)^{-\frac{1}{2}} \tag{6}$$

3.3 Density functional theory calculated band structures

Density functional theory (DFT) is a computational modeling method used to investigate the electronic structure of many-body quantum mechanical systems. DFT is commonly used in band structure calculation [8] [9] [10] and in condensed matter physics in general.

3.3.1 Comparison with 3D spectrum

In Schuster et al. [4], DFT was used to calculate the 3D q-JDOS spectrum of hexagonal boron nitride (h-BN). By extracting the (k, ϵ) points from their band structure, we can calculate the 1D q-JDOS along the MK high symmetry line. Thereafter we can compare these two spectra to see if this 1D approach can recreate some of the full 3D structures. The band structure calculated by Schuster et al. is presented in figure Figure 1, where the region of interest is marked.

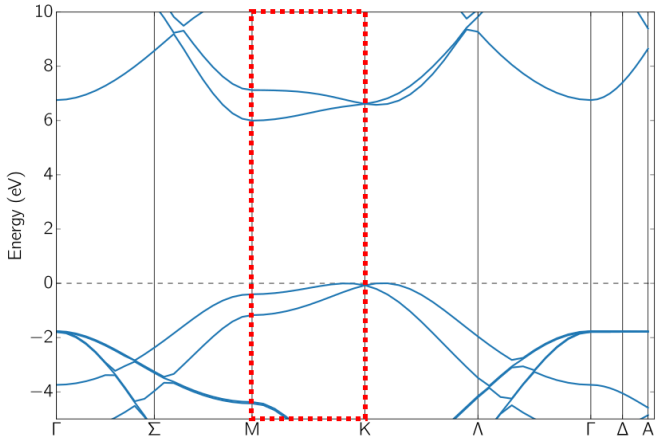

Figure 1: DFT calculated band structure of h-BN from Schuster et al. Our area of interest, the MK symmetry line, is marked by a red box.

3.3.2 Materials Project

From the Materials Project (MP) [5], DFT calculated band structures can be extracted for a numerous amount of different materials. Trough the `pymatgen`-API [11], energies and k-points along high-symmetry lines in the Brillouin zone can extracted. The k-points connecting the high symmetry points are very sparse, so cubic spline interpolation has been used to increase the k-point density. It should be noted that DFT underestimates the true band gap of materials [12]. This however can be solved by a applying a scissor operator, shifting the energy difference between the VBM and CBM to fit experimental data. The data is also given in fractional coordinates, and a transformation operation is needed to transform the k-points to Cartesian coordinates. This is explained in appendix C, with the transformation matrix from eq. (11) used.

Using the MP data, we will investigate the q-JDOS spectrum of two semiconductors. Firstly we will look at ZnO. This is a semiconductor with a direct band gap (located at the Γ point), with a hexagonal crystalline system. The Brillouin zone and band structure are shown in Figure 2 (a) and (b) respectively. To adjust DFT calculated band structure, the experimental value from [13] was used, where the band gap was determined to be $E_g = 3.37$ eV. Secondly we will look at r-SnO_2. This is also a semiconductor with a direct band gap, but with a tetragonal crystalline system. The Brillouin zone and band structure is presented in Figure 2 (c) and (d) respectively. Here we will try to determine the band gap using experimental spectra obtained from EELS.

3.4 Electron energy loss spectroscopy

By accelerating electrons with a narrow energy range, these can be pointed at a thin sample. Inbound electrons will interact with the sample by a number of different mechanisms. Measuring the energy of the outgoing electrons, one can calculate the electron energy loss after passing through the sample. Using a strong magnetic field (magnetic prism) perpendicular to the outgoing electrons, they can be separated as a function of their energies. This gives an electron intensity as a function of energy loss. The interaction between the inbound electrons and sample undergoes two types of scattering, *elastic* and *inelastic*. Elastic scattered electrons, often called forward scattered, corresponds to electrons that interact with the sample in such a way that the outgoing electrons have no energy loss. In the energy loss spectrum this will be a sharp intensity peak centred at 0, with a spread corresponding to the energy spread of the incident beam, appropriately named the zero loss peak (ZLP). The ZLP should be extracted from the spectrum, where the first width half maximum (FWHM) often is used as the energy resolution. Inelastic scattered electrons corresponds to electrons that loose energy after passing through the sample. The cause of inelastic scattering is attributed to more than a hand-full of effects such as phonon excitation, plasmon excitation, Cherenkov radiation, band transitions and more. Among these effects we will try to extract the band gap. The momentum transfer between the incident electrons and electrons in the sample is dependent on the scattering angle. By careful placement of the spectrometer entrance aperture one can single out different scattering angles and thus get different EEL spectra for different ranges of momentum transfers. For a more comprehensive explanation of momentum resolved EELS and experimental setups, see [14].

To extract the band gap, we will need the 3D JDOS for direct band gap materials. Integrated over momentum transfers, the JDOS follows the proportionality [15]:

$$\text{JDOS} \propto \sqrt{E - E_g} \tag{7}$$

By fitting eq. (7) to the lowest momentum ranges of the EELS spectra, we will use the determined band gap value E_g to adjust the DFT calculated band structure. Thereafter we will try to use the same proportionality to fit higher momentum ranges. By fitting the 1D JDOS proportionality from eq. (6) to the q-JDOS spectra at the same momentum ranges, we can see if there is some qualitative correlation between the two approaches. The experimental spectra are subject to large signal-to-noise ratio, especially for high momentum values. This causes the issue that trying to extract fine details (band gaps) can be problematic, since small energy intervals must often be considered when fitting eq. (7). To help the fitting procedure a Savitzky–Golay filter will be applied to the experimental spectra in an attempt to smooth out the noise while still maintaining as much fine structures as possible.

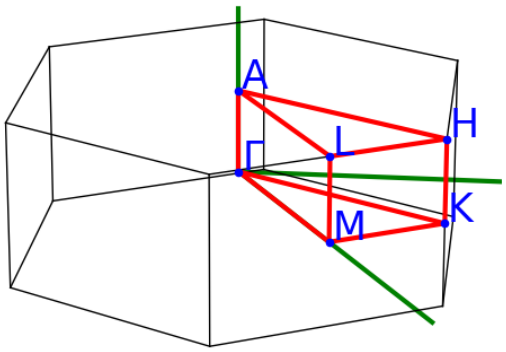

(a) ZnO Brillouin zone

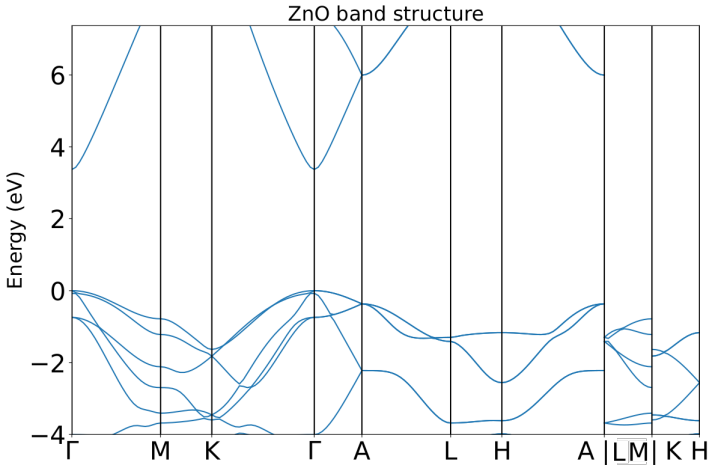

(b) ZnO band structure

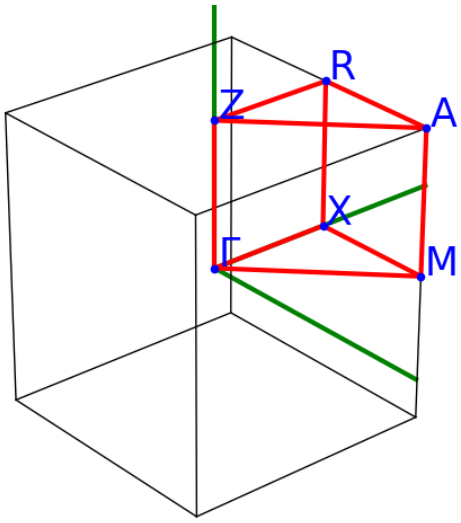

(c) r-SnO_2Brillouin zone

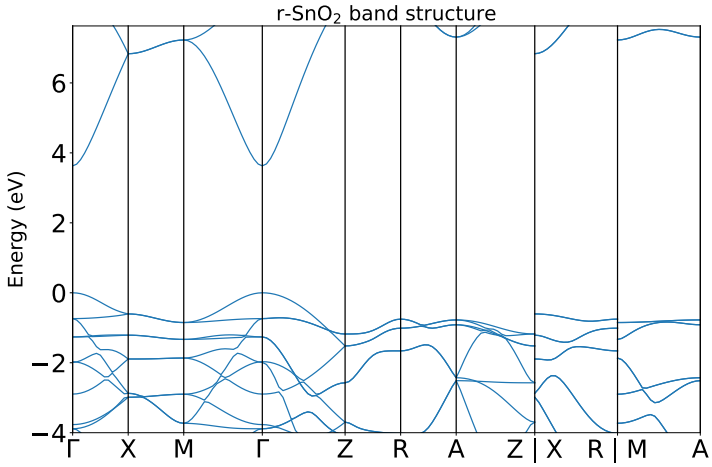

(d) r-SnO_2band structure

Figure 2: Brillouin zone and band structure for Zno and r-SnO_2. (a) Brillouin zone for ZnO. (b) Band structure of ZnO. Band gap is located at the Γ point. The q-JDOS will then be calculated for the $K\Gamma$ and ΓA lines. (c) Brillouin zone for r-SnO_2. (d) Band structure of r-SnO_2. Band gap is located at the Γ point. The q-JDOS will be calculated for the ΓZ and ΓX lines.

4 Results

4.1 Band structure modeling

Presented in Figure 3, q-JDOS and the corresponding band structure is shown for a direct gap of $E_g = 1$ eV between two parabolic bands with equal effective mass $m^* = 0.5$.

Taking the q-JDOS from Figure 3, we extract the spectrum at $q = 0$. Using this spectrum, we fit the proportionality from eq. (6). This is presented in Figure 4. With the fit restricted to the inverse square root, the band gap estimate was computed to $E_g = 0.9997$ eV with a coefficient variance of $\sigma_E^2 = 7.51 \cdot 10^{-9}\text{eV}^2$. Loosening the fit to an arbitrary exponent, the computed band gap was $E_g = 0.998$ eV with a coefficient variance of $\sigma_E^2 = 2.36 \cdot 10^{-8}\text{eV}^2$. The resulting best coefficient was estimated to be $n = -0.505$ with a coefficient variance of $\sigma_n^2 = 1.87 \cdot 10^{-6}$.

Presented in Figure 5, the q-JDOS and corresponding band structure of a indirect band gap is shown. The band gap is set at $E_g = 1$ eV between the VBM located at 0.4 $\text{Å}^{-1}$and the CBM at 0.8 Å^{-1}. The effective masses of the two bands are set equal at $m^* = 0.5$. For k-points sampling, the range has been increased to compensate due to the horizontal displacement of the indirect gap and consequently the q-range used in the JDOS calculations has also increased.

By the use of eq. 2 we can add bands that diverge from the parabolic shape when moving away from its extremal points. Another VB is added to the band structure from Figure 3, with a maximum at $(0.4\ \text{Å}^{-1}, -0.2\ \text{eV})$. The effective mass

was set to $m^* = 0.75$ making the band less steep, with $\alpha = 0.5$ eV^{-1} making the band quite linear when moving away from $k_0 = 0.4$ Å^{-1}. The band structure and the resulting q-JDOS is presented in Figure 6.

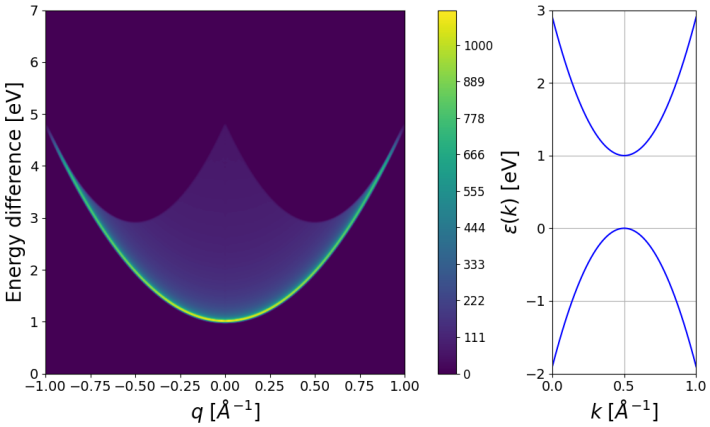

Figure 3: q-JDOS and corresponding band structure. Right: q-JDOS for energy and momentum limits $E \in [0, 7]$ eV and $q \in [-1, 1]$ Å^{-1}, with bin sizes at $\delta E = 1.4 \cdot 10^{-2}$ eV, $\delta q = 4 \cdot 10^{-3}$ Å^{-1}. Smoothed with a Gaussian filter with $\sigma = (1$ Å$^{-1}, 1$ eV). Left: Parabolic band structure with a direct band gap of $E_g = 1$ eV located at $k_0 = 0.5$ Å^{-1}. Both bands were sampled from $k \in [0, 1]$ Å^{-1}with 3000 points each.

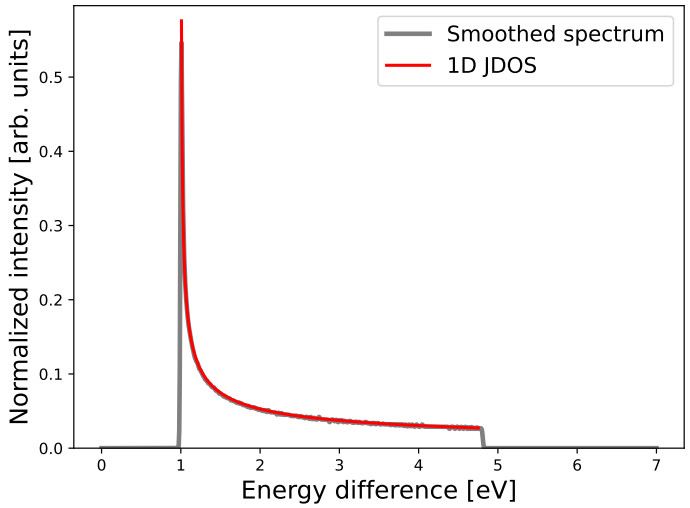

Figure 4: Normalized intensity spectrum of the q-JDOS from Figure 3, with the proportionality from eq. (6) fitted. Nonlinear least squares was used for fitting on $E \in [1, 4.75]$ eV.

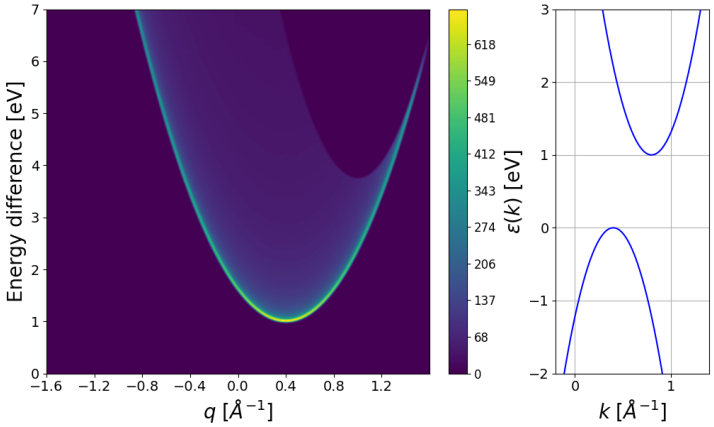

Figure 5: q-JDOS and corresponding band structure. Right: q-JDOS for energy and momentum limits $E \in [0, 7]$ eV and $q \in [-1.6, 1.6]$ Å^{-1}, with bin sizes at $\delta E = 1.4 \cdot 10^{-2}$ eV, $\delta q = 4 \cdot 10^{-3}$ Å^{-1}. Smoothed with a Gaussian filter with $\sigma = (1$ Å$^{-1}, 1$ eV). Left: Parabolic band structure with an indirect band gap of $E_g = 1$ eV between the VBM at $k_0 = 0.4$ Å^{-1}and the CBM at $k_1 = 0.8$. Both bands were sampled from $k \in [-0.2, 1.4]$ Å^{-1}with 3000 points each.

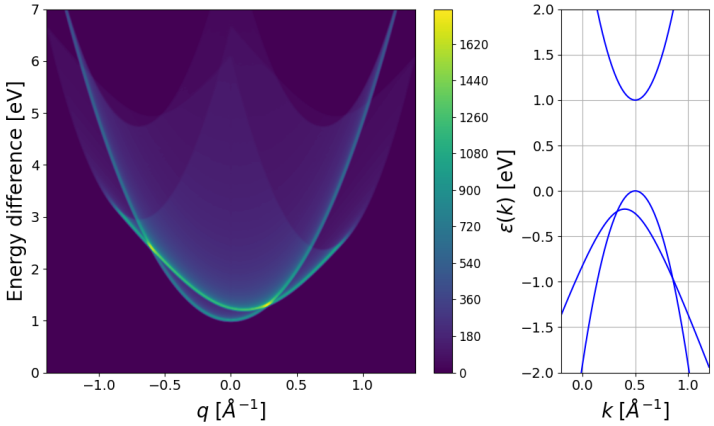

Figure 6: Same structure as in Figure 3, but an additional VB centered at $k = 0.4$. Energy and momentum limits set at $E \in [0, 7]$ eV and $q \in [-1.2, 1.2]$ Å^{-1}with bin sizes at $\delta E = 1.4 \cdot 10^{-2}$ eV and $\delta q = 5.6 \cdot 10^{-3}$ Å^{-1}. All bands were sampled from $k \in [-0.2, 1.2]$ Å^{-1}with 3000 points each.

4.2 Band structures from density functional theory

The q-JDOS computed along the MK direction using the h-BN band structure (from Figure 1) is presented in Figure 7. Only 2 VBs and 2 CBs were used for calculation, as this seems to be the approach Schuster et al. has used. All bands were interpolated using cubic splines with 3000 points. For comparison the absolute value of the momentum transfer was used.

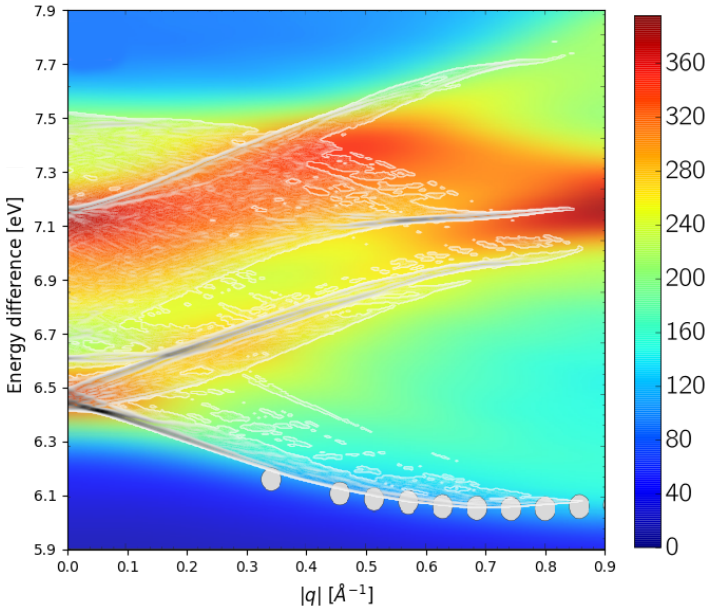

Figure 7: Showing two different JDOS calculations from the MK direction of the band structure from Figure 1. The blue to red density plot is from Schuster et al. while the gray overlaying density is calculated from the method presented here. Energy and momentum bin sizes set to $\delta E = 4.2 \cdot 10^{-3}$ eV and $\delta q = 3.6 \cdot 10^{-3}$ Å^{-1}, smoothed using a Gaussian filter with $\sigma = (1$ Å^{-1}, 1 eV).

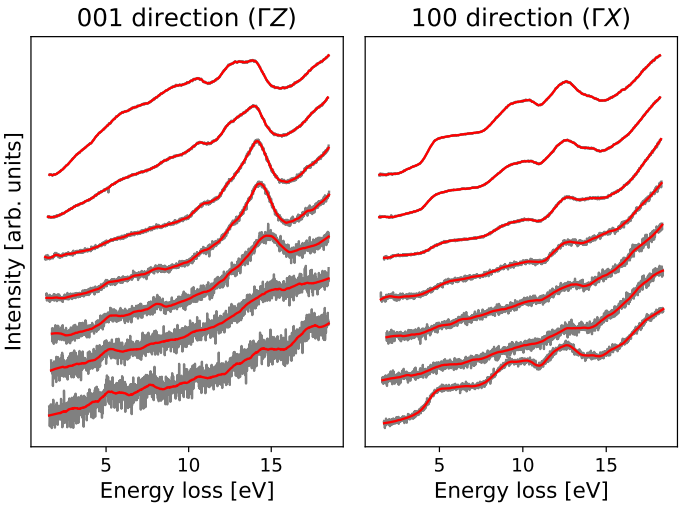

Figure 8: EEL intensity spectra for the 001 (ΓZ) direction and 100 (ΓX) direction as a function of energy loss, after the ZLP has been removed. Gray lines are the raw spectra, while the red lines are the Savitzky–Golay smoothed spectra used for fitting. The momentum range increases from top to bottom, with the 001 direction corresponding to the first column in Table 1 and the 100 direction to the first column of Table 2. The different spectra have been shifted along the y-axis for clarity.

4.2.1 Comparing r-SnO_2 energies between DFT and experimental spectra

In Figure 8 the EEL spectra for different momentum ranges are shown. From [16] the 001 and 100 directions correspond to ΓZ and ΓX respectively. These were smoothed using a Savitzky–Golay filter and fitted using the proportionality from eq. (7). The length of the fitted interval as well as computed E_g and coefficient variance is shown in Table 1 and Table 2 for the 001 (ΓZ) and 100 (ΓX) directions respectively. Using the lowest momentum range $(0 - 0.1)$ the DFT band structures were adjusted to the fitted band gap. Using the proportionality from eq. (6) the q-JDOS spectra over the same momentum ranges were fitted. This is presented in Figure 9 and Figure 10 for the 001 (ΓZ) and 100 (ΓX) directions respectively. It should also be noted that the first Brillouin zone for the ΓX direction only stretches to ≈ 0.65 Å^{-1}, about half of the largest momentum range experimentally measured for this direction. Due to this the q-JDOS spectrum has been mirrored around $q = 0.65$ Å^{-1}, explaining the fall in energy after $q = 0.75$ Å^{-1}in Figure 10.

q [Å^{-1}]	E_{int} [eV]	E_g [eV]	σ_E^2 [eV^2]
0-0.1	0.90	3.63	$5.33 \cdot 10^{-5}$
0.1-0.2	0.90	3.80	$1.81 \cdot 10^{-4}$
0.2-0.3	0.72	4.04	$3.00 \cdot 10^{-4}$
0.3-0.4	0.70	4.71	$1.42 \cdot 10^{-3}$
0.5-0.6	0.65	5.84	$7.01 \cdot 10^{-4}$
0.7-0.8	0.68	6.78	$1.58 \cdot 10^{-3}$
0.9-1.0	0.65	7.58	$1.70 \cdot 10^{-3}$

Table 1: Showing the interval length used for the fit, computed E_g and coefficient variance at different q ranges for the 001 (ΓZ) direction.

q [Å^{-1}]	E_{int} [eV]	E_g [eV]	σ_E^2 [eV^2]
0-0.1	0.88	3.84	$2.56 \cdot 10^{-5}$
0.1-0.2	0.70	3.87	$2.66 \cdot 10^{-5}$
0.2-0.3	0.70	3.89	$1.94 \cdot 10^{-5}$
0.4-0.5	0.67	5.68	$1.34 \cdot 10^{-4}$
0.7-0.8	0.66	6.35	$3.93 \cdot 10^{-4}$
0.9-1.0	0.69	4.65	$4.15 \cdot 10^{-4}$
1.2-1.3	0.80	3.78	$5.26 \cdot 10^{-6}$

Table 2: Same as Table 1 but for the 100 (ΓX) direction.

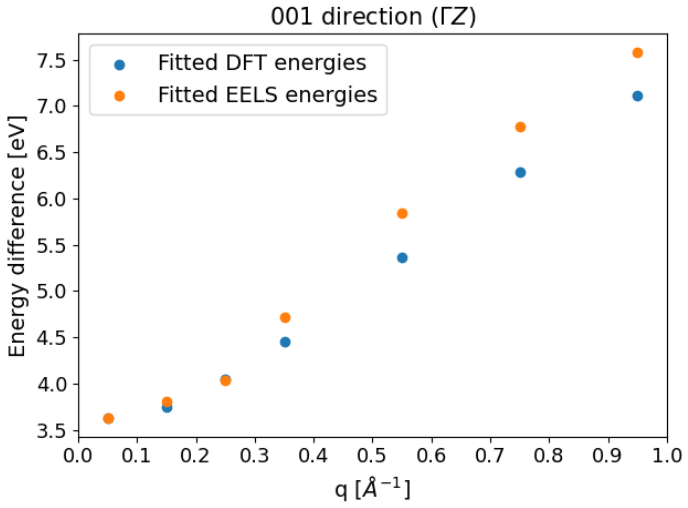

Figure 9: Comparison of energies at different q ranges fitted from EELS and calculated DFT spectra for the 001 (ΓZ) direction. The points has been placed in the middle of their respective q ranges.

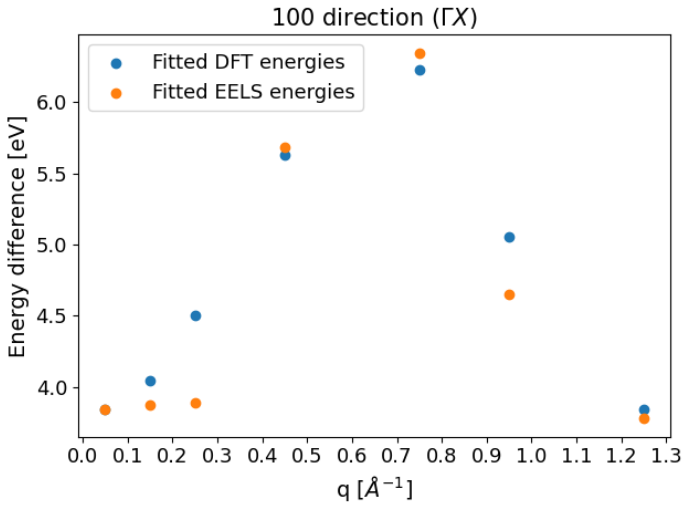

Figure 10: Same as Figure 9, but for the 100 (ΓX) direction. Note that above 0.65 Å^{-1}momentum transfers bypasses the first Brillouin zone.

4.2.2 ZnO and r-SnO_2 q-JDOS

After the DFT band structure had been adjusted to fit experimental data, the q-JDOS for the $K\Gamma$ and Γ was calculated. The result is seen in Figure 11. From the band structures in Figure 2 (b) and (d), one the lowest energy CB and the 8 lowest energy VBs were included for minimizing the energy spread in the q-JDOS for both directions (for both ZnO and r-SnO_2). For easier comparison, the energy limits for directions (for both ZnO and r-SnO_2) has been set to $E \in [2.5, 10]$ eV. The momentum limits are set to the edge of the first Brillouin zone.

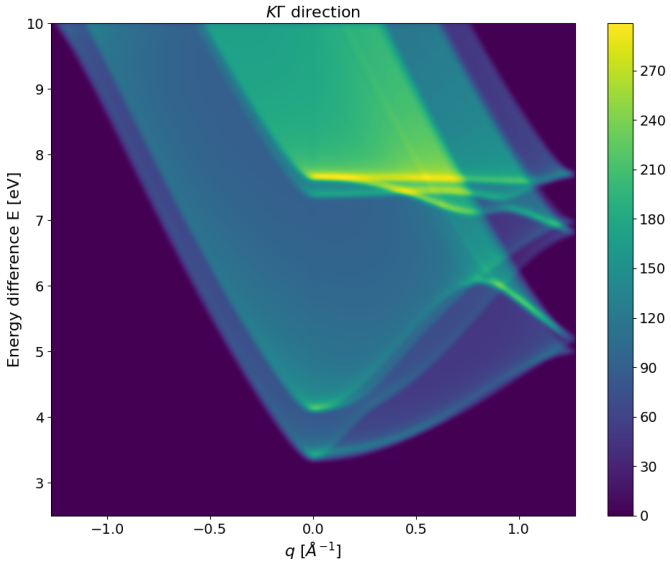

(a) ZnO $K\Gamma$

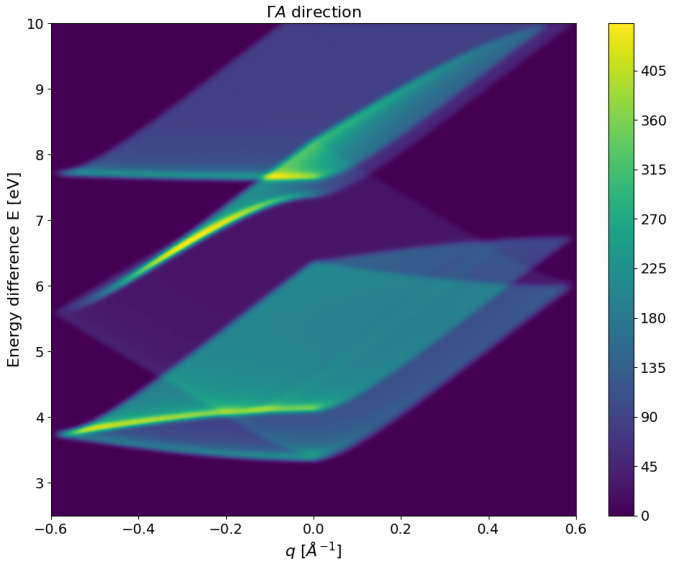

(b) ZnO ΓA

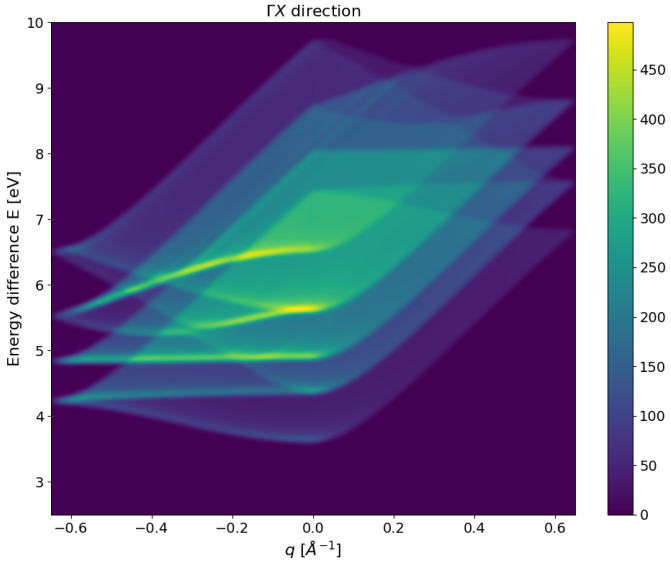

(c) r-SnO_2 ΓX

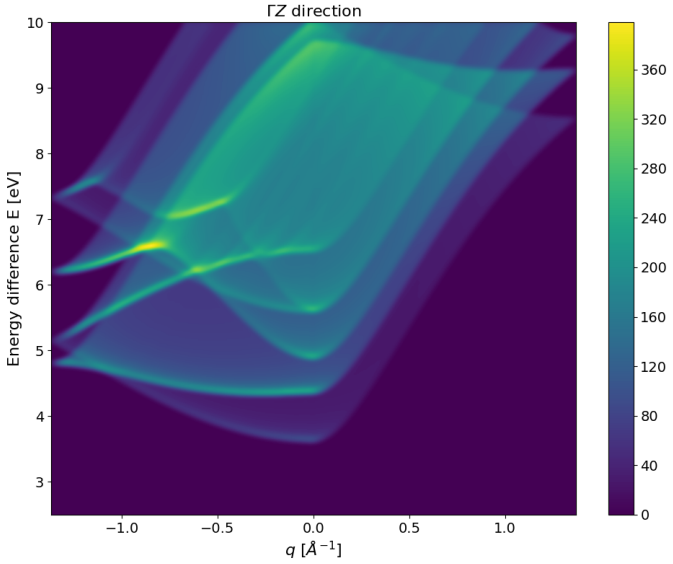

(d) r-SnO_2 ΓZ

Figure 11: q-JDOS spectra of ZnO and r-SnO_2. ZnO band transitions in the (a) $K\Gamma$ direction and (b) ΓA direction. r-SnO_2band transitions in the (c) $K\Gamma$ direction and (d) ΓA direction. Energy and momentum bin sizes set at $\delta E = 1.5 \cdot 10^{-2}$ eV and $\delta q = 2.4 \cdot 10^{-3}$ Å^{-1}.

5 Discussion

5.1 Direct and indirect band gaps

The q-JDOS from the direct band gap from Figure 3 correctly identifies the band gap at $E_g = 1$ eV with no momentum transfer. At $q = 0$ we see that transitions range from the $E \in [1, 5]$ eV. This corresponds with what we expect in the band structure, where direct transitions can happen from the VBM to CBM, all the way up to transitions from the bottom of the VB to the top of the CB. There is also a corresponding intensity decrease. This can be attributed the both bands increasing in steepness when moving away from the VBM and CBM. Since the steepness increases, the energy difference between different transitions will also increase. This in turn results in fewer states being considered equal (belonging to the same δE bin). The most prevalent feature is the high intensity parabolic line starting at $(0\ \text{Å}^{-1}, 1\ \text{eV})$ and ending at $(\pm 1\ \text{Å}^{-1}, \sim 5\ \text{eV})$. Lines such as this is a recurring feature of the 1D q-JDOS spectra. Here the attributing factors are two fold, with both transitions from the VBM to any point in the CB and transitions from any point in the VB to the CBM contributing. The common factor between these two types of transitions is that either the VBM or CBM is involved. Around these areas, the bands are much flatter than any other regions and thus the difference in band energies $\epsilon(k)$ is much smaller. When we surpass energies of these types of transitions ($E > 3$ eV), the lines fade out due to the density of $\epsilon(k)$ points becoming smaller. It should also be noted that the q-JDOS is symmetric around $q = 0$. This is due to the band structure being symmetric around the Γ point.

The fitted spectrum of the direct band gap at $q = 0$ is seen in Figure 4. Both in the inverse square root and the free exponential fit we arrived very close to the expected value of 1 eV, deviating by $3 \cdot 10^{-4}$ eV and $2 \cdot 10^{-3}$ eV respectively. Both these values are safely below the energy bin size at $\delta E = 1.4 \cdot 10^{-2}$, giving good reassurance that the implementation works as expected. In addition the free exponential fit gave a proportionality constant of $n = -0.505$, very close to the expected value of -0.5.

The indirect band gap structure from Figure 5 does share quite a lot of features with the direct case. With the band gap identified at $E_g = 1$ eV with $q = 0.4$ Å^{-1}, the high intensity parabolic line is identical to that of the direct case and simply shifted to $q = 0.4$ Å^{-1}. However for this indirect case, the q-JDOS is not symmetric around the band gap momentum transfer ($q = 0.4$ Å^{-1}). For $q > 0.4$ Å^{-1}transitions, the high intensity line fades away at $(1.6\ \text{Å}^{-1}, 6\ \text{eV})$. Since the bands are sampled from the same k-points with a center at $k = 0.6$ Å^{-1}, the VB goes deeper down the energy range right of the VBM than left of the VBM (and correspondingly CB higher up the energy range left of the CBM than right of the CBM). Thus the largest positive momentum transfer will have a lower energy difference than the largest negative momentum transfer. There is also a fading of the high intensity line for $q < 0.4$, but as stated this happens at much larger energy differences and is not present inside the energy limits used for the q-JDOS calculations.

The addition of a non parabolic VB to the band structure with a direct band gap is seen in Figure 6. Adding another band introduces another high intensity line, again mimicking the shape of the VB. The lowest point along this line is located at $(0.1\ \text{Å}^{-1}, 1.2\ \text{eV})$, corresponding to a transition from the top of the non parabolic band to the CBM. In the band structure the two VBs overlap at approximately $(0.33\ \text{Å}^{-1}, -0.22\ \text{eV})$ and $(0.87\ \text{Å}^{-1}, -1\ \text{eV})$. Transitions from these points to the CBM is the two areas of highest intensity in the q-JDOS located at around $(0.28\ \text{Å}^{-1}, 1.29\ \text{eV})$ and $(0.58\ \text{Å}^{-1}, 2.38\ \text{eV})$

5.2 Comparison with Schuster et al.

In figure Figure 7 we see the comparison of the 3D q-JDOS calculations of h-BN with the 1D calculations along the MK symmetry line. Both density plots identify the band gap at around $E_g = 6$ eV for a momentum transfer of $q = 0.7$ Å^{-1}. The calculations presented here seems to capture some of the structure presented in the full 3D q-JDOS, with high intensity areas traced out. However there are some clear differences present. The full 3D calculations have a much wider range of energies for every q transitions. This is probably due to the 3D case calculating every transition that is parallel to the MK direction in the Brillouin zone, not just transitions on the high symmetry line. The 1D q-JDOS might be considered as a thin slice of the full 3D structure. In addition the 3D structure does not suffer from the apparent fading of the state density present in the 1D calculations. Unfortunately this is a by-product of the 1D model and is present in every q-JDOS calculation presented here. If the k-point spacing of bands are equal with n_k points, there will always be n_k transitions with $q = 0$. The smallest momentum transfer (not considering absolute value) will have $n_k - 1$ transitions and so on until the largest momentum transfer that spans the whole Brillouin zone with 1 possible transition. Possible approaches to circumnavigate this have been tried, such as random point sampling and weighting of different q values, but non was found to produce any reasonable improvement.

5.3 DFT and EELS comparison of r-SnO_2 energies

In Figure 9 and Figure 10, the energies obtained by fitting the EELS and DFT spectra are compared for different q values. There are some qualitative similarities worth mentioning. For the 001 (ΓZ) direction from Figure 9, both DFT and EELS energies increases with higher momentum ranges. The slope of the increase seems to be relatively equal, with the experimental values increasing slightly faster with q. The 100 (ΓX) direction seen in Figure 10 on the other hand has poorer correspondence, though the overstepping of the first Brillouin zone seems to agree between EELS and DFT. The first three points corresponding to momentum transfers of $(0 - 0.1)$ Å^{-1}, $(0.1 - 0.2)$ Å^{-1}and $(0.2 - 0.3)$ Å^{-1}results in approximately equal energies from the EEL spectra, while the q-JDOS spectra seems to overestimate these. One explanation for this may be the limited momentum resolution in EELS. The spectrometer entrance aperture has a fixed

momentum resolution and can overlap between different momentum ranges. EELS intensities is in general proportional to q^{-2} [17] [18]. Thus if the measured momentum ranges overlap even slightly, features from lower momentum ranges will transfer over to higher momentum ranges. Of course the fact that the q-JDOS spectra have been calculated only using k-points along the high symmetry line also neglects a lot of the complexities of the band structure, such that these lower energy transitions for $(0.1-0.2)$ Å^{-1}and $(0.2-0.3)$ Å^{-1}might be attributed to transitions between states elsewhere in the Brillouin zone.

There are some complications when using the proportionality from eq. (5). It is only valid for parabolic bands when integrated over all momentum transfers. From the band structure in Figure 2 (d) the VB and CB for both ΓZ and ΓX seems fairly parabolic (keeping in mind that we are only seeing the 1D slice of the full 3D band structure). Applying the method for specific q-ranges is problematic, but results from [19] have shown that this method might hold some merit. There is also a problem with the robustness of the method. As the EEL spectra does not exclusively contained the band gap (as previously discussed) a selected part of the spectrum must be fitted. This does unfortunately bring on some variability in the result, as exemplified in Figure 12.

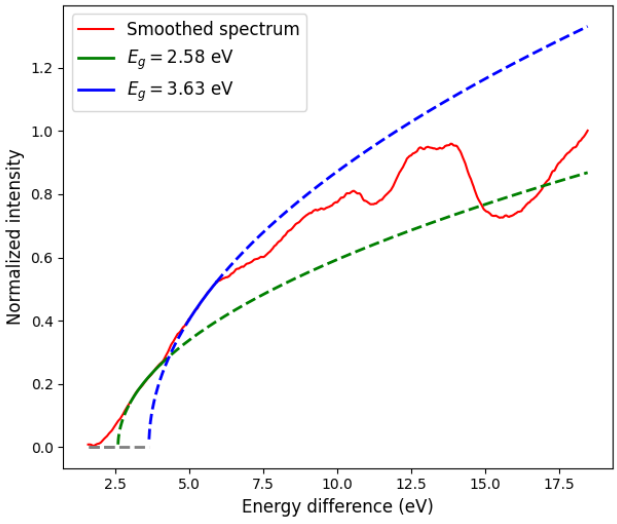

Figure 12: Showing two different fits for the 001 (ΓZ) direction of r-SnO_2in the $0-0.1$ Å^{-1}momentum range. As seen both fits are preformed on energy intervals relatively close together, but results in two different E_g values. Here the fit in blue ($E_g = 3.64$ eV) was chosen due to a lower coefficient variance.

The subjectivity of the fitting procedure used here does bring on some variability of the results. By use of eq. (7), the determined coefficient E_g will always be smaller than the lower bound of the fitting range and thus a systematic shifting of fitting intervals to higher energies has been preformed with increasing momentum transfers. Other methods are in practice preformed [20], but resides outside the scope of material presented here.

When fitting the 100 (ΓX) direction, the experimental momentum ranges exceeds that of the first Brillouin zone. The X point is located at $k \approx 0.65$ Å^{-1}relative to the Γ point and thus has a maximum momentum transfer of $q = 0.65$ Å^{-1}. Since the experimental spectra contains up to and including $(1.2-1.3)$ Å^{-1}, the measured values spans approximately the first and seconds Brillouin zone. To mediate this, the calculated q-JDOS was mirrored around the X point, such that the Γ point of the second Brillouin zone is located at $k \approx 1.3$Å^{-1}relative to the first Γ point. This explains the decrease in energy shown in Figure 10 around $q \approx 0.65$ Å^{-1}.

5.4 ZnO q-JDOS

The q-JDOS for ZnO along the $K\Gamma$ and ΓA direction can be seen in Figure 11 (a) and (b) respectively. For both spectra the lowest energy transition is identified at $E_g = 3.37$ eV for $q = 0$, in correspondence with the energy shift following the use of the scissor operator. In the $K\Gamma$ direction, we observe that for negative q transitions the energy difference increases quickly. This is due to CB growing quickly in energy when approaching the K point. It seems that due to the steepness of this CB, the shape of the VB is more arbitrary than that of the positive q transitions.

For positive q transitions however, the band shapes are more apparent in the q-JDOS. This can be attributed to transitions going from a point in one of the VBs to the CBM, similarly to what was observed for the idealized band structures. Going all the way from $q = 0$ to $q = 1.3$ Å^{-1}, this traces out the shape of each VB. A similar argument can be made by transitions to higher points in the CB. When moving away from the CBM the transition energies increases while the range of momentum transfers decreases. This creates the characteristic "shadows" above each high intensity line.

In the ΓA direction, the band structure from Figure 2 (b) shows a greater spread of VB energies compared with the $K\Gamma$ direction. This is clearly seen in the q-JDOS, where the spread in energy from the two lowest high intensity lines to the two highest is very large. The two lowest high intensity lines starting at $(-0.6$ Å$^{-1}, 3.9$ eV) and ending at $(0, 4.1$ eV$)/(0, 3.37$ eV) are attributed to transitions from the two high energy valence bands meeting at the A point to the CBM.

5.5 r-SnO_2 q-JDOS

In Figure 11 (c) and (d) the q-JDOS for r-SnO_2 along the ΓZ and ΓX direction is presented. Both these directions has a contrast to that of ZnOs $K\Gamma$ direction (Figure 11 (a)), in that most of the structure in the q-JDOS can be seen on the negative instead of the positive q direction. This is simply a product of how the high symmetry lines are traversed (going from Γ to Z instead of Z to Γ) and is left untouched for easier compartment with the band structures from Figure 2 (b) and (d).

Similarly for what we saw for ZnO, both the r-SnO_2 ΓX and ΓZ directions shows high intensity lines following transitions from an arbitrary state in the VB to the CBM. Looking at the band structure for the ΓX direction in Figure 2 (d), we see many VBs merging together at the X point. In the q-JDOS this can also be seen for momentum transfers around $q \approx -0.65$ Å^{-1}. When moving towards momentum transfers $q > -0.65$Å^{-1}these high intensity lines split before reaching $q = 0$ where they again merge. This also reflects the band structure where bands merge together when reaching the Γ point. Similarly the ΓZ direction shares some of this merging and splitting, but it is less present in both the band structure and q-JDOS.

6 Conclusion

The numerical study of the q-JDOS was successfully implemented, in good agreement with the analytical result for a direct transition. Investigation of both normal and perturbed parabolic band structures showed that the main features of the q-JDOS follows transitions from the VBs to the CBM closely. Comparing the 1D q-JDOS of h-BN with the full 3D calculations, we saw that some of the main features were captured. Despite this the energy density spread, especially for higher momentum transfers, were lacking due to only sampling a small subspace of the full Brillouin zone. The comparison between energy shifted DFT calculated spectra showed good qualitative agreement with the experimental values for r-SnO_2along the 001 and 100 direction, despite the simplicity of the model and complications related to fitting experimental spectra. The calculated q-JDOS spectra for r-$SnO_2$and ZnO gave some insight in how the shape of band structures shape the transition space, but mostly showed the same main features as the idealized band structures.

The natural next step would be to expand the model to a 3D Brillouin zone. This would allow for calculating transitions not only along high symmetry lines, but all $\mathbf{q}$ vectors parallel to a high symmetry line. Preforming these calculations for material band structures requires development of a DFT simulation, a task both difficult and lengthy.

A Derivation of 1D JDOS for parabolic bands

We aim to calculate the theoretical JDOS for parabolic 1D bands for $q = 0$. From [21] we express the volume Ω_n of an n-dimensional k-space as.

$$\Omega_n(k) = c_n k^n \tag{8}$$

Where c_n is the length/area/volume of the n-dimensional unit sphere, with k as the maximum allowed wave vector. For our 1D model, the length on the unit sphere is $c_1 = 2$ [22]. The number of possible energies E inside an interval $[E, E + \mathrm{d}E]$, the density of state, then follows as.

$$D_n(E) = \frac{\mathrm{d}\Omega_n(E)}{\mathrm{d}E} \tag{9}$$

In general every transition between the VB and CB can result in a momentum change. Thus we consider a state in the VB with an initial wave vector k_i and energy $\epsilon_v(k_i)$, undergoing a transition to a state in the CB with a wave vector k_f and energy $\epsilon_c(k_f)$. We call the wave vector transfer between the two states $q = k_f - k_i$. Solving for k_f, we can express the energy difference between the CB and VB states as a function of the initial momentum.

$$\epsilon_c(k_i) - \epsilon_v(k_i) = \epsilon_c + \frac{\hbar^2(k_i + q)^2}{2m_c^*} - \left(\epsilon_v - \frac{\hbar^2 k_i^2}{2m_v^*}\right)$$

We then rename $k_i \to k$ for clarity and reduce to the $q = 0$ case. Thereafter defining energy difference as $E = \epsilon_c(k) - \epsilon_v(k)$ and the band gap $E_g = \epsilon_c - \epsilon_v$ as the minimum energy difference. In addition by defining a 'mean' effective mass $m_\mu^* = m_c^* m_v^*/(m_c^* + m_v^*)$ we arrive at.

$$E - E_g = \frac{\hbar^2 k^2}{m_\mu^*}$$
$$k = \frac{\sqrt{m_\mu^*(E - E_g)}}{\hbar}$$

Inserting this equation for the wave vector into the k-space volume from eq. (8) with $c_n = 2$ and preforming the derivative in (9) we arrive at the joint density of state.

$$D(E) = \frac{\sqrt{m_\mu^*}}{\hbar}(E - E_g)^{-\frac{1}{2}} \tag{10}$$

B q-JDOS implementation pseudo code

Here a short pseudo code of the implemented algorithm for computing the q-JDOS is presented. This assumes that every state below the ϵ_F is stored in β, while every state above ϵ_F is stored in α. Here we also allow for α and β to have different k-points (energy evaluated at different points). When this is not the case, the same k-point spacing can be used for all states to save memory (only a problem when many bands are considered).

Initialize: $q_{min}, q_{max}, E_{min}, E_{max}, \delta E, \delta q$

$n_q = \lfloor (q_{max} - q_{min})/\delta q \rfloor$
$n_E = \lfloor (E_{max} - E_{min})/\delta E \rfloor$

$J = (n_E, n_q)$ integer matrix

for $i = 0, ..., n_k$ **do**
  for $j = 0, ..., n_k$ **do**

    $q = \alpha.k[j] - \beta.k[i]$
    $E = \alpha.\epsilon[j] - \beta.\epsilon[i]$

    if $q \notin [q_{min}, q_{max}]$ or $E \notin [E_{min}, E_{max}]$ **then**
      Do nothing
    else
      $k = \lfloor (q - q_{min})/\delta q \rfloor$
      $l = \lfloor (E - E_{min})/\delta E \rfloor$
      $J[k, l]$ += 1
    end if
  end for
end for

C Conversion from fractional coordinates

The DFT calculated data from MP is given in fractional coordinates. This means that coordinates are given as fractions of the Brillouin Zone primitive vectors, and are thus unit-less. A general k-point in reciprocal space can the be expressed as.

$$\mathbf{k} = h\mathbf{a} + k\mathbf{b} + l\mathbf{c}$$

Where (h, k, l) are the unit-less fractional coordinates, which MP uses as a basis for its k-points. To transform these to Cartesian coordinates, we have to multiply the (h, k, l) fractional coordinates by a transformation matrix U give by [23][24].

$$U = \begin{pmatrix} a & b\cos\gamma & c\cos\beta \\ 0 & b\sin\gamma & c\frac{\cos\alpha - \cos\beta\cos\gamma}{\sin\gamma} \\ 0 & 0 & \frac{\Omega}{ab\sin\gamma} \end{pmatrix} \tag{11}$$

Where $a = |\mathbf{a}|$, $b = |\mathbf{b}|$ and $c = |\mathbf{c}|$ and α, β and γ are the angles between $(\mathbf{b}, \mathbf{c})$, $(\mathbf{a}, \mathbf{c})$ and $(\mathbf{b}, \mathbf{c})$ respectively. Here we have made use of Ω , the volume of the Brillouin Zone unit cell, given by.

$$\Omega = \mathbf{a} \cdot (\mathbf{b} \times \mathbf{c})$$
$$= abc\sqrt{1 - \cos^2\alpha - \cos^2\beta - \cos^2\gamma + 2\cos\alpha\cos\beta\cos\gamma}$$

References

[1] A. Yoshikawa, H. Matsunami, and Y Nanishi. *Wide Bandgap Semiconductors. Development and Applications of Wide Bandgap Semiconductors*. springer, 2007, p. 2. ISBN: 978-3-540-47235-3.

[2] R.U. Martinelli and D.G. Fisher. "The application of semiconductors with negative electron affinity surfaces to electron emission devices". In: *Proceedings of the IEEE* 62.10 (1974), pp. 1339–1360. DOI: 10.1109/PROC.1974.9626.

[3] M. P. Mikhailova, K. D. Moiseev, and Yu. P. Yakovlev. "Discovery of III–V Semiconductors: Physical Properties and Application". In: *Semiconductors* 53.3 (2019), pp. 273–290. ISSN: 1090-6479. DOI: 10.1134/S1063782619030126. URL: https://doi.org/10.1134/S1063782619030126.

[4] R. Schuster et al. "Direct observation of the lowest indirect exciton state in the bulk of hexagonal boron nitride". In: *Physical Review B* 97.4 (2018). ISSN: 2469-9969. DOI: 10.1103/physrevb.97.041201. URL: http://dx.doi.org/10.1103/PhysRevB.97.041201.

[5] Anubhav Jain et al. "The Materials Project: A materials genome approach to accelerating materials innovation". In: *APL Materials* 1.1 (2013), p. 011002. ISSN: 2166532X. DOI: 10.1063/1.4812323. URL: http://link.aip.org/link/AMPADS/v1/i1/p011002/s1\&Agg=doi.

[6] Charles Kittel. *Introduction to solid state physics*. eng. 8th ed. Hoboken, N.J: Wiley, 2005. ISBN: 9780471415268.

[7] Daniel V Schroeder. *An Introduction to Thermal Physics*. eng. Oxford: Oxford University Press, 2021, p. 267. ISBN: 9780192895547.

[8] M. Hussein. N. Assadi and Dorian A. H. Hanaor. "Theoretical study on copper's energetics and magnetism in TiO2 polymorphs". In: *Journal of Applied Physics* 113.23 (2013), p. 233913. ISSN: 1089-7550. DOI: 10.1063/1.4811539. URL: http://dx.doi.org/10.1063/1.4811539.

[9] Ángel Morales-García, Rosendo Valero, and Francesc Illas. "An Empirical, yet Practical Way To Predict the Band Gap in Solids by Using Density Functional Band Structure Calculations". In: *The Journal of Physical Chemistry C* 121.34 (2017), pp. 18862–18866. ISSN: 1932-7447. DOI: 10.1021/acs.jpcc.7b07421. URL: https://doi.org/10.1021/acs.jpcc.7b07421.

[10] A.A. Lavrentyev et al. "Electronic structure and optical properties of Cs2HgI4: Experimental study and band-structure DFT calculations". In: *Optical Materials* 42 (2015), pp. 351–360. ISSN: 0925-3467. DOI: https://doi.org/10.1016/j.optmat.2015.01.026. URL: https://www.sciencedirect.com/science/article/pii/S0925346715000543.

[11] Shyue Ping Ong et al. "Python Materials Genomics (pymatgen): A robust, open-source python library for materials analysis". In: *Computational Materials Science* 68 (2013), pp. 314–319. ISSN: 0927-0256. DOI: https://doi.org/10.1016/j.commatsci.2012.10.028. URL: https://www.sciencedirect.com/science/article/pii/S0927025612006295.

[12] John P. Perdew et al. "Understanding band gaps of solids in generalized Kohn–Sham theory". In: *Proceedings of the National Academy of Sciences* 114.11 (2017), 2801–2806. ISSN: 1091-6490. DOI: 10.1073/pnas.1621352114. URL: http://dx.doi.org/10.1073/pnas.1621352114.

[13] Norlida Kamarulzaman, Muhd Firdaus Kasim, and Roshidah Rusdi. "Band Gap Narrowing and Widening of ZnO Nanostructures and Doped Materials". In: *Nanoscale Research Letters* 10.1 (2015), p. 346. ISSN: 1556-276X. DOI: 10.1186/s11671-015-1034-9. URL: https://doi.org/10.1186/s11671-015-1034-9.

[14] F. S. Hage et al. "Topologically induced confinement of collective modes in multilayer graphene nanocones measured by momentum-resolved STEM-VEELS". In: *Phys. Rev. B* 88 (15 2013), p. 155408. DOI: 10.1103/PhysRevB.88.155408. URL: https://link.aps.org/doi/10.1103/PhysRevB.88.155408.

[15] B. Rafferty and L. M. Brown. "Direct and indirect transitions in the region of the band gap using electron-energy-loss spectroscopy". In: *Phys. Rev. B* 58 (16 1998), pp. 10326–10337. DOI: 10.1103/PhysRevB.58.10326. URL: https://link.aps.org/doi/10.1103/PhysRevB.58.10326.

[16] Maofeng Dou and Clas Persson. "Comparative study of rutile and anatase SnO2 and TiO2: Band-edge structures, dielectric functions, and polaron effects". In: *Journal of Applied Physics* 113 (Feb. 2013). DOI: 10.1063/1.4793273.

[17] R. J. Nicholls et al. "Theory of momentum-resolved phonon spectroscopy in the electron microscope". In: *Phys. Rev. B* 99 (9 2019), p. 094105. DOI: 10.1103/PhysRevB.99.094105. URL: https://link.aps.org/doi/10.1103/PhysRevB.99.094105.

[18] R. F. Egerton. *Electron Energy-Loss Spectroscopy in the Electron Microscope*. 2nd ed. Edmonton Alberta Canada: Springer, 1986, p. 170.

[19] Bilden S. R. *Master's Thesis: Simulation of momentum resolved Electron Energy Loss Spectroscopy in the low loss region using model band structures*. 2018.

[20] Mirjana Dimitrievska et al. "The Advantage of Nanowire Configuration in Band Structure Determination". In: *Advanced Functional Materials* n/a.n/a (), p. 2105426. DOI: https://doi.org/10.1002/adfm.202105426. eprint: https://onlinelibrary.wiley.com/doi/pdf/10.1002/adfm.202105426. URL: https://onlinelibrary.wiley.com/doi/abs/10.1002/adfm.202105426.

[21] R. J Elliott. *An introduction to solid state physics and its applications*. eng. London, 1974.

[22] Harley Flanders. *Differential forms with applications to the physical sciences*. eng. New York, 1989.

[23] J. L. Sussman et al. "A structure-factor least-squares refinement procedure for macromolecular structures using constrained and restrained parameters". In: *Acta Crystallographica Section A* 33.5 (1977), pp. 800–804. DOI: https://doi.org/10.1107/S0567739477001958. eprint: https://onlinelibrary.wiley.com/doi/pdf/10.1107/S0567739477001958. URL: https://onlinelibrary.wiley.com/doi/abs/10.1107/S0567739477001958.

[24] M. G. Rossmann and D. M. Blow. "The detection of sub-units within the crystallographic asymmetric unit". In: *Acta Crystallographica* 15.1 (1962), pp. 24–31. DOI: https://doi.org/10.1107/S0365110X62000067. eprint: https://onlinelibrary.wiley.com/doi/pdf/10.1107/S0365110X62000067. URL: https://onlinelibrary.wiley.com/doi/abs/10.1107/S0365110X62000067.